

MIT Open Access Articles

Relative efficiency of land surface energy balance components

The MIT Faculty has made this article openly available. **Please share** how this access benefits you. Your story matters.

Citation: Bateni, S. M., and D. Entekhabi. "Relative Efficiency of Land Surface Energy Balance Components." *Water Resources Research* 48.4 (2012). Copyright 2012 by the American Geophysical Union

As Published: <http://dx.doi.org/10.1029/2011wr011357>

Publisher: American Geophysical Union (AGU)

Persistent URL: <http://hdl.handle.net/1721.1/77890>

Version: Final published version: final published article, as it appeared in a journal, conference proceedings, or other formally published context

Terms of Use: Article is made available in accordance with the publisher's policy and may be subject to US copyright law. Please refer to the publisher's site for terms of use.



Relative efficiency of land surface energy balance components

S. M. Bateni¹ and D. Entekhabi¹

Received 3 September 2011; revised 6 February 2012; accepted 2 March 2012; published 11 April 2012.

[1] The partitioning of available energy into dissipative fluxes over land surfaces is dependent on the state variable of the surface energy balance (land surface temperature) and the state variable of the surface water balance (soil moisture). The direct measurement of the turbulent fluxes is achieved with in situ instruments at tower sites. These point-scale measurements are sparsely distributed. Broader scale mapping of the turbulent fluxes is mostly dependent on land surface temperature (LST) and optical/infrared vegetation that can be sensed remotely. There are several data assimilation approaches currently in use that intake sequences of daytime LST that attain different diurnal amplitudes depending on available energy and the relative efficiency of surface energy balance to infer the magnitude of surface flux components such as latent and sensible heat flux. In this study we perform stability analysis on the evolution of LST in order to provide insights into the physical bases for why LST variations can be used to diagnose surface energy balance (SEB) components. The derived relative efficiencies of SEB components in dissipating available energy at the land surface are tested using two field experiment measurements. The results show that the theoretically derived relative efficiencies of SEB components agree well with field observations. The study provides insight into how LST sequences implicitly contain the signature of partitioning of available energy among SEB components and can be used to infer their magnitudes.

Citation: Bateni, S. M., and D. Entekhabi (2012), Relative efficiency of land surface energy balance components, *Water Resour. Res.*, 48, W04510, doi:10.1029/2011WR011357.

1. Introduction

[2] The sensible (H), latent (LE), and ground (G) heat fluxes as well as outgoing longwave radiation (OLR) are key terms in the surface energy balance and work to dissipate available energy at the land surface. The magnitude of the combined turbulent fluxes ($H + LE$) and their relative partitioning affect the evolution of surface heating and drying, influence the structure of boundary layer clouds and act to force the dynamics of the lower troposphere. Ground heat flux has a direct and significant influence on soil temperature which affects the rates of biochemical processes. The components of surface energy balance (SEB) are routinely observed at select point locations where instruments are installed on tower platforms (e.g., AmeriFLUX, FLUXNET). The networks of such tower sites are however limited in coverage and mapping important fluxes such as H and LE is not possible based on their observations alone. Remote sensing data do have the advantage of spatial coverage. However they cannot be used to sense fluxes directly. Related variables such as land surface temperature (LST), optical/infrared vegetation indices (VI) and soil moisture are nevertheless observed using remote sensing instruments. There are many proposed approaches for using LST, VI, soil moisture and other directly sensed variables to estimate

the SEB components and especially the turbulent fluxes. They may be broadly categorized in three main groupings.

[3] In the first grouping, empirical relations have been formed between remotely sensed LST, VI and the turbulent fluxes [Moran *et al.*, 1994; Gillies *et al.*, 1997; Sandholt *et al.*, 2002; Kalma *et al.*, 2008]. A prime example of such approaches is the so-called triangle method [e.g., Gillies *et al.*, 1997; Carlson, 2007] for retrieving surface evaporation rate from the normalized difference vegetation index (NDVI)-LST relationship.

[4] Beyond these empirical and site-specific approaches, a second group of flux retrieval models mostly use instantaneous observations of LST combined with surface air micrometeorology measurements to solve the surface energy balance and predict surface heat fluxes [Anderson *et al.*, 1997; Bastiaanssen *et al.*, 1998a, 1998b; Mecikalski *et al.*, 1999; Jiang and Islam, 2001; Su, 2002; Kalma *et al.*, 2008]. Sensible heat flux (H) is related to LST. Net radiation (R_n) is estimated by establishing a balance between the incoming and outgoing longwave and shortwave radiation. These models are diagnostic and often require closure assumptions since both the land surface temperature (T) and its time tendency (dT/dt) appear in the surface energy balance equation. The most common closure assumption is that the ground heat flux (G) that is related to time tendency (dT/dt) is a given empirical fraction of the net radiation, i.e., $G/R_n = \text{constant}$, or a function of vegetation indices [Santanello and Friedl, 2003]. Given estimates of H , R_n , and G , latent heat flux (LE) may be then obtained as the residual of the surface energy balance.

¹Ralph M. Parsons Laboratory, Massachusetts Institute of Technology, Cambridge, Massachusetts, USA.

[5] The evolution of LST implicitly contains information about the history of partitioning among the surface energy balance components including the turbulent fluxes. This is because different components of SEB have different relative efficiencies in dissipating available energy at the land surface. This recognition has led to a third grouping of approaches to inferring LE and H from remote sensing data. Sequences of LST measurements are assimilated into the force-restore equation to estimate evaporative fraction, $EF = LE/(LE + H)$ (which scales partitioning among the turbulent heat fluxes) and bulk heat transfer coefficient, C_{HN} (that scales the sum of turbulent heat fluxes, $H + LE$) [Caparrini *et al.*, 2003, 2004a, 2004b; Crow and Kustas, 2005; Sini *et al.*, 2008]. This group of studies is built based on the principle that EF is almost constant during daytime hours in cloud-free days with intense solar radiation forcing [Lhomme and Elguero, 1999; Gentine *et al.*, 2007, 2011].

[6] The diurnal cycle of solar radiation provides a strong forcing of the surface energy balance. Components of the surface energy balance such as latent heat flux, sensible heat flux, ground heat flux and outgoing longwave radiation work to dissipate the available energy at the land surface. Since they have different relative efficiencies, the diurnal cycle of land surface temperature will be affected if there are controls and limits on the fluxes. For example low turbulence can limit the sum of the sensible and latent heat fluxes; moisture limitation can affect the partitioning among the sensible and latent heat fluxes. Thus sensing of the diurnal cycle of land surface temperature, coupled with knowledge of the radiative forcing of the land surface can yield important information on the magnitude of the surface energy balance components. The key enabling factor is the existence of differences in the relative efficiencies of the components of surface energy balance. In this study we derive the theoretical relative efficiencies and estimate their relative magnitudes.

[7] Linear stability analysis is used to quantify the relative efficiencies of the surface energy balance components. In the linear stability analysis, LST perturbations to the stable (reference) state are applied to a linearized form of the dynamic equation governing LST evolution (surface energy balance). The theoretical relative efficiencies obtained from stability analysis are evaluated for two field experiment data sets.

2. Stability Analysis

[8] The one-dimensional vertical heat diffusion equation in a soil column is

$$c \frac{\partial T_s(z, t)}{\partial t} = p \frac{\partial^2 T_s(z, t)}{\partial z^2} \quad (1)$$

with boundary conditions

$$\begin{aligned} \lim_{z \rightarrow \infty} T_s(z, t) &= \bar{T} \\ -p \frac{\partial T}{\partial z}(0, t) &= G(t), \end{aligned} \quad (2)$$

where $T_s(z, t)$ is soil temperature at depth z and time t , \bar{T} is the deep ground temperature, p is the soil thermal conductivity, and c is the volumetric heat capacity. $G(t)$ is the

ground heat flux or surface boundary forcing, and is related to the other components of the land surface energy balance via,

$$G = R_n - H - LE, \quad (3)$$

where R_n is the net radiation. Each term in (3) is generally related to land surface temperature, $T(0, t)$, and each term dissipates LST perturbations and restores the system to equilibrium. The question is how each term is effective and influential in this process. Linear stability analysis addresses this question by providing insight into the contribution of each of the terms in dissipating LST perturbations.

[9] To implement the stability analysis, the solution to the system (1)–(3) may be approximated at the surface by a single ordinary differential equation. This approximation allows modeling the evolution of land surface temperature in response to variations in surface boundary forcing $G(t)$ occurring at a principal diurnal frequency (ω). To achieve this approximation, the following assumptions are invoked: (1) the surface forcing term $G(t)$ has a strong single-frequency (e.g., diurnal) behavior in time, and (2) the soil thermal properties are nearly constant with depth [Dickinson, 1988; Hu and Islam, 1995; Castelli *et al.*, 1999]. This approximation is represented by the well-known force-restore equation for land surface temperature, which consists of a forcing term (1st on the right hand side, that takes into account the effect of surface energy budget) and a restoring term (2nd on the right side, accounts for the effect of deep ground temperature \bar{T}) [Dickinson, 1988; Hu and Islam, 1995; Gao *et al.*, 2008; Campo *et al.*, 2009]:

$$\frac{dT_s}{dt} = \frac{\sqrt{\omega}}{P} [R_n - H - LE] - \omega(T_s - \bar{T}), \quad (4)$$

where P is the thermal inertia, $\sqrt{pc/2}$.

[10] Net radiation, the forcing in (4), is the sum of the incoming and outgoing shortwave and longwave radiation fluxes:

$$R_n = (1 - \alpha)R_s^\downarrow + R_l^\downarrow - \varepsilon\sigma T_s^4, \quad (5)$$

where α is the surface albedo, R_s^\downarrow is the incoming solar radiation, R_l^\downarrow is the incoming longwave radiation, ε is the surface emissivity and $\sigma = 5.67 \times 10^{-8} \text{ (W m}^{-2} \text{ K}^{-4})$ is the Stefan-Boltzmann constant.

[11] Using a bulk resistance formulation, sensible heat flux can be expressed in terms of the near surface gradient of temperature (T) from the land surface (subscript s) to the atmosphere (subscript a):

$$H = \frac{\rho c_p}{r_a} (T_s - T_a), \quad (6)$$

where c_p is the air specific heat, ρ is the air density, T_a is the air temperature at a reference height z_{ref} , and r_a is the aerodynamic resistance for heat transfer from the surface to the overlying air layer at z_{ref} .

[12] When soil or vegetation do not exert control or resistance on evaporation (as in the case of moist soil or

well-watered vegetation), LE is at its maximum possible value denoted by potential evaporation,

$$LE_p = \frac{\rho L}{r_a} (q_s^*(T_s) - q_a), \quad (7)$$

where $q_s^*(T_s)$ is the saturated specific humidity at the surface temperature (T_s), q_a is the overlying air humidity and L is the specific latent heat of vaporization. This is a conceptual flux and only an intermediary step toward characterizing the actual latent heat flux.

[13] The actual evaporation term (LE) is reduced below the potential value through a moisture availability parameter (β) that is dependent on soil moisture or vegetation stress. This term links the surface energy balance to the surface water balance [Mahfouf and Noilhan, 1991]:

$$LE = \beta LE_p. \quad (8)$$

As mentioned above, β depends on soil moisture but it has some important limitations. Carlson *et al.* [2007] shows that vegetation reduces transpiration below potential even when the soil is adequately moist. Here β is a bulk parameter used to indicate either drier soils or stressed vegetation that reduce evaporation below its potential value.

[14] Substituting (5)–(8) in (4) results in

$$\begin{aligned} \frac{dT_s}{dt} = \frac{\sqrt{\omega}}{P} \left((1 - \alpha)R_s^\downarrow + R_l^\downarrow - \varepsilon\sigma T_s^4 - \frac{\rho c_p}{r_a} (T_s - T_a) \right. \\ \left. - \beta \frac{\rho L}{r_a} (q_s^*(T_s) - q_a) \right) - \omega (T_s - \bar{T}). \end{aligned} \quad (9)$$

[15] The outgoing longwave radiation ($\varepsilon\sigma T_s^4$) and saturated specific humidity ($q_s^*(T_s)$) terms are linearized around air temperature (T_a) through truncated Taylor's series,

$$\begin{aligned} \frac{dT_s}{dt} = \frac{\sqrt{\omega}}{P} \left((1 - \alpha)R_s^\downarrow + R_l^\downarrow + 3\varepsilon\sigma T_a^4 - 4\varepsilon\sigma T_a^3 T_s - \frac{\rho c_p}{r_a} (T_s - T_a) \right) \\ + \frac{\sqrt{\omega}}{P} \left(-\beta \frac{\rho L}{r_a} (q_s^*(T_a) + \left. \frac{\partial q_s^*}{\partial T_s} \right|_{T_a} (T_s - T_a) - q_a) \right) - \omega (T_s - \bar{T}). \end{aligned} \quad (10)$$

[16] The linearized LST evolution equation can be regrouped into terms, with and without T_s :

$$\frac{dT_s}{d\tau} = - \left(\beta \frac{\Delta}{\gamma} T_s + T_s + \frac{r_a}{r_g} T_s + \frac{r_a}{r_o} T_s \right) + \mathcal{Q}', \quad (11)$$

where

$$\tau = \frac{t}{Pr_a / \sqrt{\omega} \rho c_p}, \quad (12)$$

(τ is the nondimensional time scale);

$$r_o = \frac{\rho c_p}{4\varepsilon\sigma T_a^3}, \quad (13)$$

(r_o is radiative flux resistance);

$$\gamma = \frac{c_p P_a}{0.622L}, \quad (14)$$

(γ is Psychometric constant);

$$\Delta = \frac{de_s}{dT_s}, \quad (15)$$

(Δ is Clausius – Calpeyron relation);

$$r_g = \frac{\rho c_p}{P\sqrt{\omega}}, \quad (16)$$

(r_g is ground heat flux resistance);

$$\begin{aligned} \mathcal{Q}' = \frac{(1 - \alpha)R_s^\downarrow + R_l^\downarrow}{\rho c_p / r_a} + T_a \left(1 + \frac{3\varepsilon r_a}{4r_o} \right) \\ - \beta \frac{L}{c_p} q_s^*(T_a) + \beta \frac{\Delta}{\gamma} T_a + \beta \frac{L}{c_p} q_a + \frac{P\sqrt{\omega} r_a \bar{T}}{\rho c_p}, \end{aligned} \quad (17)$$

\mathcal{Q}' contains all the terms that do not have an explicit dependence on the state variable, T_s . P_a is the air pressure, and e_s is the saturated air vapor pressure.

[17] The system is strictly dissipative since all the state-dependent terms are always negative. The system tends to restore to an equilibrium surface temperature, T_s^* . At this equilibrium, $dT_s/d\tau|_{T_s=T_s^*} = 0$. Writing (11) in terms of deviations from T_s^* , and defining the perturbation $\delta T_s = T_s - T_s^*$ yields:

$$\frac{d\delta T_s}{d\tau} = - \left(\beta \frac{\Delta}{\gamma} + 1 + \frac{r_a}{r_g} + \frac{r_a}{r_o} \right) \delta T_s. \quad (18)$$

The solution of (18) is

$$\delta T_s(\tau) = \delta T_s(0) e^{-\beta \frac{\Delta}{\gamma} \tau} e^{-\tau} e^{-\frac{r_a}{r_g} \tau} e^{-\frac{r_a}{r_o} \tau}, \quad (19)$$

where $\delta T_s(0)$ is an initial land surface temperature perturbation due to anomalies in available energy as included in \mathcal{Q}' .

[18] Two important dependencies have been neglected in this linearization in order to simplify the problem and hence focus on the more major relations. The nondimensional time τ includes the turbulent flux aerodynamic resistance (r_a). This resistance is dependent on the factors that affect turbulence in the surface air layer. Besides the wind shear near the surface, gradients in air temperature also affect the static stability, buoyancy and ultimately turbulence in the air above the surface [Liu *et al.*, 2007]. This dependence on temperature is not explicitly factored in the above analysis. Furthermore, the ground heat flux resistance (r_g) depends on soil thermal inertia, which varies slightly with soil moisture content. This dependence is also not factored in explicitly.

3. Discussion

[19] Equation (19) indicates that the initial land surface temperature perturbation, $\delta T_s(0)$, is reduced in time by four dissipative mechanisms: (1) latent heat flux, (2) sensible

heat flux, (3) ground heat flux, and (4) outgoing longwave radiation. The relative efficiency and effectiveness of these mechanisms may be assessed through four nondimensional measures $\beta \frac{\Delta}{\gamma}$ (latent heat flux relative efficiency), 1 (sensible heat flux relative efficiency), $\frac{r_a}{r_g}$ (ground heat flux relative efficiency), and $\frac{r_a}{r_o}$ (outgoing longwave radiation relative efficiency). The nondimensional efficiency terms are relative to sensible heat flux which is unity due to the linear dependence in (6). The efficiency terms depend on a number of environmental and physiographic factors but air temperature, i.e., climate, is a common and principal factor.

[20] Figure 1 shows how each of the four mechanisms (or components of SEB) influences the dissipation of available energy at the land surface at different air temperatures. For a moist surface where β is near unity, latent heat flux efficiency ($\frac{\Delta}{\gamma}$ or the nondimensional Clausius-Clapeyron relation) is a strong function of air temperature. It is important to note that in colder climates when air temperature is low, sensible heat flux is more efficient than latent heat flux. Therefore, over cold surfaces such as polar oceans, the Bowen ratio (H/LE) is often large and even greater than unity. Between 0°C and 25°C, $\frac{\Delta}{\gamma}$ ranges between 0.66 (less than one) and 2.84 (larger than one). This significant increase of the latent heat flux efficiency ($\frac{\Delta}{\gamma}$) over only a limited air temperature range is due to the nonlinear dependence of saturated vapor pressure (e_s) on the air temperature, which is governed by the Clausius-Clapeyron relationship.

[21] The nonlinear dependence of saturated specific humidity ($q_s^* \approx 0.622 \frac{e_s}{P_a}$) with respect to air temperature (Figure 2) is well known to be the physical basis for the dependence of the Bowen ratio on air temperature over moist surfaces (energy-limited evaporation regime or unstressed evaporation). *Monteith* [1981] (source for Figure 2) shows

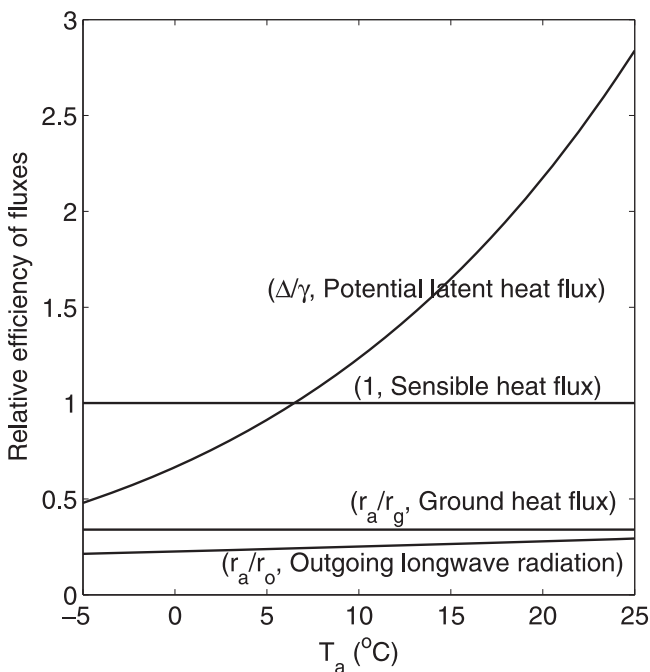


Figure 1. Relative efficiency of different fluxes versus air temperature.

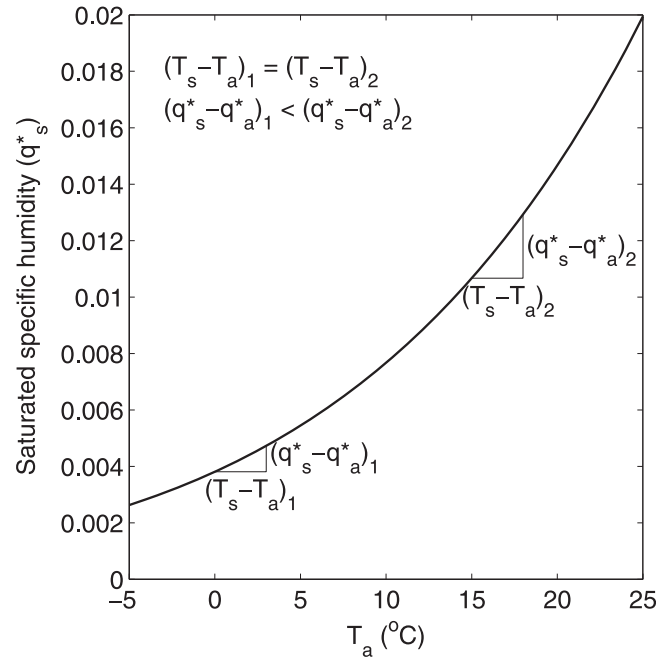


Figure 2. Variation of saturated specific humidity with air temperature [after *Monteith*, 1981].

that the efficiency of latent heat flux increases rapidly as the temperature rises. The quantity $dq_s^*/dT_s|_{T_a}$ (slope of air saturated specific humidity-temperature dependence and related to Clausius-Clapeyron relation) increases with air temperature. Therefore, the same $(T_s - T_a)$ that scales sensible heat flux magnitudes at different temperatures result in very different $(q_s^* - q_a^*)$ values that drive the latent heat flux (Figure 2). As a result, over a reasonable air temperature range latent heat flux varies from less to more efficient than sensible heat flux in dissipating heat. *Monteith* [1981] shows the nonlinear dependence of saturated specific humidity ($q_s^* \approx 0.622 \frac{e_s}{P_a}$) on air temperature (Figure 2), indicating that LE is more efficient than H , especially at higher temperatures. However, his study did not provide insight on the relative efficiency of other components of the SEB equation (e.g., ground heat flux and outgoing longwave radiation).

[22] Generally during midday and near the peak of solar forcing when the energy balance components generally take on their maximum values, $\frac{r_a}{r_o}$ and $\frac{r_a}{r_g} \approx O(10^{-1} \text{ to } 1)$ and hence the two turbulent heat flux mechanisms (sensible and latent heat flux) are more efficient compared to outgoing longwave radiation and ground heat flux. The scales $\frac{r_a}{r_o}$ and $\frac{r_a}{r_g}$ both have the same order of magnitude but usually $\frac{r_a}{r_g}$ is greater than $\frac{r_a}{r_o}$ and consequently ground heat flux is more influential than outgoing longwave radiation to restore the system to its equilibrium state.

[23] A nominal r_a value of 60 (s m^{-1}) is used to compute the relative efficiency of OLR ($\frac{r_a}{r_o}$) and ground heat flux ($\frac{r_a}{r_g}$) (Figure 1). To compute r_g (see equation (16)), soil thermal inertia (P) is set equal to a typical value of 800 ($\text{J m}^{-2} \text{K}^{-1} \text{s}^{-1/2}$). The results in Figure 1 show that among all the components of surface energy balance, outgoing longwave radiation is the least efficient and the efficiency

only slightly increases in warmer climates. The ground heat flux is also relatively inefficient when compared to the turbulent fluxes near midday and peak solar radiation hours [Gentine *et al.*, 2010]. Its efficiency does not increase with air temperature and generally is one-third less efficient than sensible heat flux during midday.

[24] The dependency of latent heat flux efficiency on air temperature for a moist surface is shown in Figure 1 and further explained with Figure 2 and accompanying discussion. Besides the latent heat flux relative efficiency dependence on air temperature, it also scales with moisture stress at the land surface through β . This is also the critical link to the surface water balance and indicates how the sequences of LST, given incoming radiation, can be used to infer attributes of the surface water balance. Figure 3 shows the sensitivity of actual latent heat flux efficiency ($\beta\Delta/\gamma$) to air temperature variations at different β values. For low β values (i.e., around 0.1), the latent heat flux efficiency increases slightly with increasing air temperature. For β values close to one, the efficiency of latent heat flux increases significantly with an increase in the air temperature. This is because β scales the relative efficiency which increases with air temperature. Figure 3 also indicates that for a given value of T_a the evaporation rate (LE efficiency) is at its peak at the first stage of evaporation (energy limited) when soil is sufficiently wet and β is close to 1. As evaporation proceeds and transitions to the second stage of evaporation (water limited), $\beta\Delta/\gamma$ decreases and evaporation (latent heat flux efficiency) is strongly restricted by the soil moisture or vegetation stress response control on moisture availability.

[25] The nominal conditions in Figure 1 correspond to midday over regions with minimal advection and cloud intermittency. The nominal case is selected to correspond with the peak solar conditions when the components of the surface energy balance are generally at their highest values.

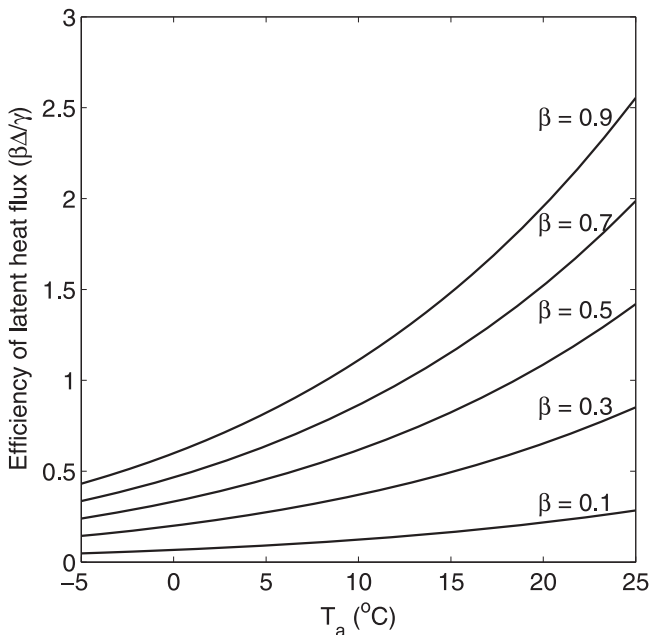


Figure 3. Efficiency of latent heat flux ($\beta\Delta/\gamma$) versus air temperature for different β values.

Nonetheless the relative efficiencies in (19) also apply to other conditions but take on different values. For example during nighttime when the air above the land surface becomes stably stratified on many occasions, the aerodynamic resistance r_a becomes large and the outgoing longwave radiation resistance r_o and ground heat flux resistance r_g are less in magnitude leading to relatively higher relative efficiencies (nondimensional $\frac{r_a}{r_o}$ and $\frac{r_a}{r_g}$ with r_a in the numerator). Hence these two fluxes dominate the surface energy balance. The relative efficiencies derived in this study are meant to provide insight into the mechanisms that enable data assimilation schemes that use sequences of daytime LST to work. Hence our focus is on the midday nominal conditions.

4. Testing With Field Observations

[26] The theoretical sensible, latent, and ground heat fluxes as well as outgoing longwave radiation relative efficiencies (1, $\beta\Delta/\gamma$, r_a/r_g , and r_a/r_o , respectively) are compared with the corresponding measurements (H/H , LE/H , G/H , and OLR/H) from two field experiments. The field experiments cover contrasting environments. The first field experiment was conducted in a subhumid environment, namely the tall grass prairie in Kansas (First ISLSCP Field Experiment, FIFE). During the FIFE experiment (summers in the May 1987 to late 1989) extensive surface micrometeorology and flux-tower observations were collected at several locations across a 15 km \times 15 km site over the Konze prairie [Sellers *et al.*, 1992]. Betts and Ball [1998] generated a site-averaged data set (referred to as the FIFE data set in this study) based upon multiple station data series. Thus the FIFE data set provides high-quality half-hourly flux, micrometeorology (wind speed, air temperature, and humidity at a reference height of 2 m), and radiometric LST data.

[27] Sud Mediterannee (SUDMED) field experiment was conducted in a semiarid region in Marrakesh, Morocco. The conditions of this experiment are described in the work of Duchemin *et al.* [2006], Gentine *et al.* [2007], and Chehbouni *et al.* [2008]. The study site used here (R3) is a wheat field with sparse vegetation. The R3 site is located 45 km east of Marrakech and covers an area of 2800 ha. Two field parcels within the R3 site, namely the 123rd (R3-B123) and 130th (R3-B130), were fully instrumented to provide continuous measurements of micrometeorological data at 2 m above the ground, heat fluxes, and LST every half an hour. The measurement period covers all cycles of wheat season: sowing, vegetative growth, full canopy, and senescence. The explored site is periodically irrigated by flooding [Gentine *et al.*, 2011]. This caused significant changes in the energy partitioning at the land surface and it is thus well-suited experiment for our study.

[28] The soil type at R3 site is mainly composed of clay and sand. The volumetric heat capacity of soil can be estimated from $c = c_s + \theta c_w$ [De Vries, 1963; Campbell, 1985] (where c_w and c_s are the volumetric heat capacity of water and dry soil, and θ is the volumetric soil water content). The literature value for c_w is 4.2×10^6 (J m $^{-3}$ K $^{-1}$) [Hillel, 1998; Abu-Hamdeh, 2003]. Following Gentine *et al.* [2011], c_s is set to 1.42×10^6 (J m $^{-3}$ K $^{-1}$). Also, the mean of volumetric soil water content (θ) measurements during the observation period is 0.28. Substituting the abovementioned

magnitudes of c_s , c_w , and θ into $c = c_s + \theta c_w$ leads to a value of 2.60×10^6 ($\text{J m}^{-8} \text{K}^{-1}$) for the soil volumetric heat capacity (c). Based on the soil type (clay and sand) and its average water content ($\theta = 0.27$), the soil heat conductivity (p) is set to 1.35 ($\text{J m}^{-8} \text{K}^{-1}$) [Hillel, 1998; Abu-Hamdeh, 2003].

[29] Figure 4 compares the theoretical relative efficiencies of H , G , OLR, and LE (i.e., 1 , r_a/r_g , r_a/r_o , and $\beta\Delta/\gamma$) with the corresponding measurements (i.e., H/H , G/H , OLR/H , and LE/H) available from FIFE and SUDMED datasets. The theoretical relative efficiencies for sensible heat flux (1), ground heat flux (r_a/r_g), and outgoing longwave radiation (r_a/r_o) are shown as solid lines. Relative efficiencies of H , G , and OLR observations (i.e., H/H , G/H , OLR/H) are indicated on the same figure by circles. The error bars are plus and minus one standard deviation for data in each T_a bin. These observed relative efficiency values are obtained at solar noon time on days with clear-sky conditions.

[30] The theoretical and observed relative efficiency of LE are classified in terms of their effective β . The LE efficiency strongly depends on β (Figure 4). Light, medium, and dark gray bands indicate the range of variability of the theoretical relative efficiency of LE (i.e., $\beta\Delta/\gamma$) for $0 < \beta < 0.3$, $0.3 < \beta < 0.6$, and $0.6 < \beta < 0.9$, respectively. Similarly, relative efficiencies of LE measurements (i.e., LE/H) are classified into three groupings according to their β values: $0 < \beta < 0.3$ (shown by triangles), $0.3 < \beta < 0.6$ (crosses), and $0.6 < \beta < 0.9$ (black circles). The observational data effective β values associated with the relative efficiency of measured LE are retrieved as the ratio of LE observations to LE_p estimations. LE_p is estimated from the Penman equation:

$$\text{LE}_p = \frac{\Delta(R_n - G) + \rho L \gamma (q_s^*(T_a) - q_a)/r_a}{\Delta + \gamma}, \quad (20)$$

where $q_s^*(T_a) = 0.622e_s/(P_a - 0.378e_s)$, and r_a is obtained by substituting the measurements of H , T_s , and T_a in equation (6).

[31] The observed efficiencies of SEB components (i.e., LE/H , H/H , G/H and OLR/H), which are represented by symbols in Figure 4 are relative to an equilibrium state where the flux and LST perturbations vanish nearly together. For example, the sensible heat flux approaches zero when the land and reference height temperatures equilibrate to the same value. Similarly, the ground heat flux vanishes when the land surface temperature approaches the deep soil temperature. The latent heat flux vanishes at a temperature that brings the specific humidity at the surface to be equal to that of air at reference height. The OLR flux is the gray body Stefan-Boltzmann law ($\epsilon\sigma T_s^4$) and as a flux does not approach zero until temperature itself is zero. A reference state needs to be defined for the OLR term near which both the heat dissipation through OLR flux and the land surface temperature perturbation generally vanish together. The equilibrium (zero) state for this flux is defined as the flux that would lead to isothermal conditions between the land and overlying air temperature. The land surface temperature perturbation would approach zero together with the OLR flux with this definition. We consider

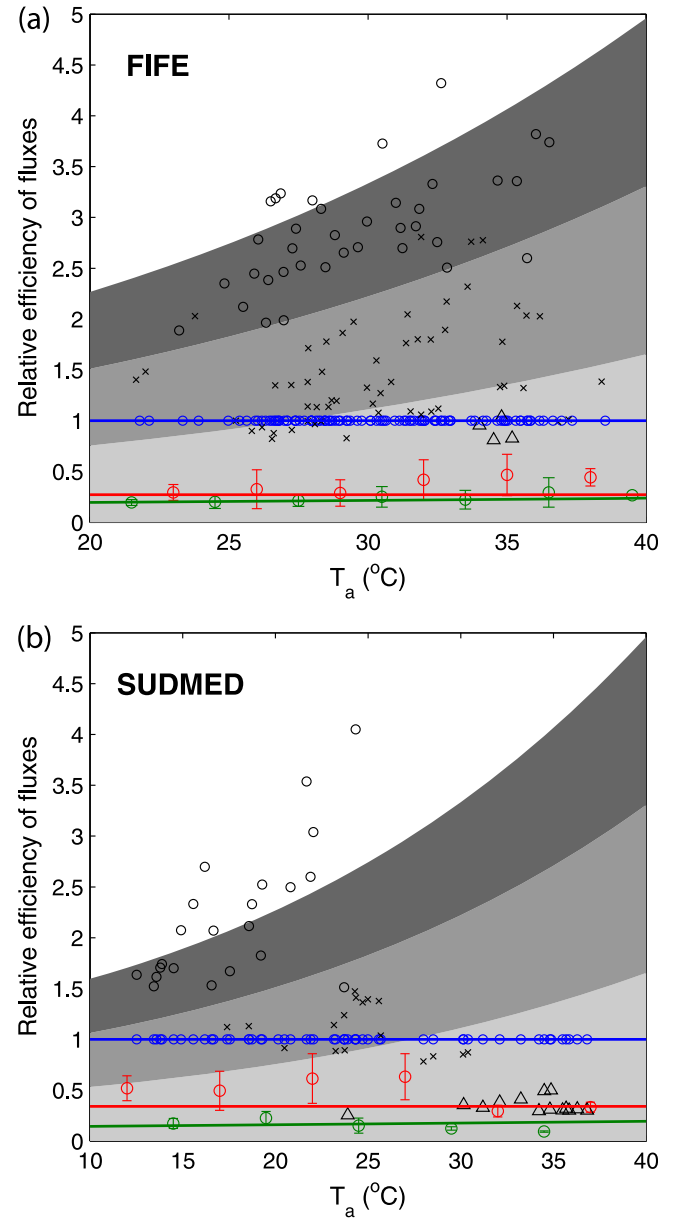


Figure 4. Comparison of theoretical relative efficiencies of H , LE , G , and OLR with measurements for (top) FIFE and (bottom) SUDMED. Theoretical efficiencies of H , G , and OLR (i.e., 1 , r_a/r_g , r_a/r_o) are shown by blue, red, and green lines, respectively. Light, medium, and dark gray bands represent the range of variability of theoretical relative efficiency of LE (i.e., $\beta\Delta/\gamma$) for $0 < \beta < 0.3$, $0.3 < \beta < 0.6$, and $0.6 < \beta < 0.9$, respectively. Observed relative efficiencies of sensible heat flux, ground heat flux, and outgoing longwave radiation (i.e., H/H , G/H , and OLR/H) are indicated by blue, red, and green circles, respectively, with 1 standard deviation variability in each T_a bin. Measured relative efficiency of latent heat flux (i.e., LE/H) are classified according to their β values: triangles ($0 < \beta < 0.3$), crosses ($0.3 < \beta < 0.6$), and black circles ($0.6 < \beta < 0.9$).

an isothermal condition between the land surface and the surface air layer as this reference state.

[32] As shown in Figure 4 the gray bands defining ranges of the latent heat flux relative efficiency correspond well

with the experimental values. The magnitudes and discrimination among them for different β values are consistent. Also, the increasing rate of $\beta\Delta/\gamma$ with air temperature at different β values is consistent with the observations. For low β values (light gray band), $\beta\Delta/\gamma$ increases slightly as air temperature rises. Similar trend is seen in the observations (triangles). In contrast, for high β values (dark gray band), $\beta\Delta/\gamma$ rises rapidly when air temperature increases. Similar pattern can be observed in the measurements (black circles). Finally the observed relative efficiencies of ground heat flux, and outgoing longwave radiation agree well in terms of magnitude and range with the corresponding theoretical values (see Figure 4).

5. Conclusion

[33] Land surface temperature temporal variations contain a significant amount of information about the partitioning of available energy among the land surface energy balance components (sensible, latent, and ground heat fluxes as well as outgoing longwave radiation). Since these dissipative terms have different relative efficiencies, the evolution of land surface temperature in response to radiative forcing contains the signature of the relative magnitude of surface energy balance components. The key enabling factor in using remotely sensed land surface temperature to estimate and map surface fluxes is the fact that differences exist in the relative efficiencies of surface energy balance components. In this study we derive these theoretical relative efficiencies of surface energy balance components. Stability analysis of surface temperature evolution is used to quantify the relative efficiency of all the surface temperature-dependent components.

[34] The results of the stability analysis show that, during daytime and near peak solar radiative forcing hours, the relative efficiency of latent heat flux varies significantly with air temperature when soil is moist or when the vegetation is unstressed. For a moist surface where β is close to unity, latent heat flux is one of the least efficient mechanisms at -5°C , while it becomes the most efficient one at about 8°C . This characteristic of latent heat flux is due to the nonlinear dependence of saturated specific humidity on air temperature. The relative efficiency of latent heat flux is also scaled by the availability of water at the land surface. Here we used an effective factor (β) to characterized the actual evaporation relative to its potential value.

[35] This study provides insights into why the sequences of LST (with temporal frequency that could characterize the diurnal cycle of LST) are often robust bases for inferring the partitioning of available energy and especially the ratio of turbulent fluxes in data assimilation (DA) systems.

Notation

c	Soil volumetric heat capacity, $\text{J m}^{-3} \text{K}^{-1}$
c_p	Specific heat of air at constant pressure, $\text{J kg}^{-1} \text{K}^{-1}$
e_s	Saturated air vapor pressure, Pa
G	Ground heat flux, W m^{-2}
H	Sensible heat flux, W m^{-2}
L	Specific latent heat of vaporization, J kg^{-1}
LE	Latent heat flux, W m^{-2}
LE _p	Potential latent heat flux, W m^{-2}

p	Soil thermal conductivity, $\text{W m}^{-2} \text{K}^{-1}$
P	Soil thermal inertia, $\text{J m}^{-2} \text{K}^{-1} \text{s}^{-1/2}$
P_a	Surface air pressure, Pa
$q_s^*(T_s)$	Saturated specific humidity at the surface temperature, kg kg^{-1}
$q_s^*(T_a)$	Saturated specific humidity at the air temperature, kg kg^{-1}
q_a	Air specific humidity, kg kg^{-1}
R_l^+	Incoming longwave radiation, W m^{-2}
R_n	Net radiation, W m^{-2}
R_s^+	Incoming solar radiation, W m^{-2}
r_a	Aerodynamic resistance for heat transfer from the surface to overlying air layer, s m^{-1}
r_g	Ground heat flux resistance, s m^{-1}
r_o	Radiative flux resistance, s m^{-1}
T_s	Land surface temperature, K
T_a	Air temperature, K
\bar{T}	Deep ground temperature, K
T_s^*	Equilibrium surface temperature, K
t	Time, s
z	Soil depth, m
z_{ref}	Height of micrometeorological measurements, m
α	Albedo
β	Evaporation reduction parameter
ω	Principal diurnal frequency of surface boundary forcing, s^{-1}
ε	Surface thermal emissivity
σ	Stefan-Boltzmann constant, $\text{W m}^{-2} \text{K}^{-4}$
ρ	Air density, kg m^{-3}
τ	Nondimensional time scale
Δ	Saturation vapor pressure gradient with temperature, Pa K^{-1}
γ	Psychrometric constant, Pa K^{-1}

References

- Abu-Hamdeh, N. H. (2003), Thermal properties of soils as affected by density and water content, *Biosyst. Eng.*, *86*, 97–102, doi:10.1016/S1537-5110(03)00112-0.
- Anderson, M. C., J. M. Norman, G. R. Diak, W. P. Kustas, and J. R. Mecikalski (1997), A two-source time-integrated model for estimating surface fluxes using thermal infrared remote sensing, *Remote Sens. Environ.*, *60*(2), 195–216, doi:10.1016/S0034-4257(96)00215-5.
- Bastiaanssen, W. G. M., M. Menenti, R. A. Feddes, and A. A. M. Holtslag (1998a), A remote sensing surface energy balance algorithm for land (SEBAL): 1. Formulation, *J. Hydrol.*, *212–213*, 198–212, doi:10.1016/S0022-1694(98)00253-4.
- Bastiaanssen, W. G. M., H. Pelgrum, J. Wang, Y. Ma, J. F. Moreno, G. J. Roerink, and T. van der Wal (1998b), A remote sensing surface energy balance algorithm for land (SEBAL): 2. Validation, *J. Hydrol.*, *212–213*, 213–229, doi:10.1016/S0022-1694(98)00254-6.
- Betts, A. K., and J. H. Ball (1998), FIFE surface climate and site-average dataset 1987–89, *J. Atmos. Sci.*, *55*, 1091–1108.
- Campbell, G. S. (1985), *Soil Physics with Basic: Transport Models for Soil-Plant Systems*, Elsevier, New York.
- Campo, L., F. Castelli, D. Entekhabi, and F. Caparrini (2009), Land-atmosphere interactions in a high resolution atmospheric simulation coupled with a surface data assimilation scheme, *Nat. Hazards Earth Syst. Sci.*, *9*, 1613–1624, doi:10.5194/nhess-9-1613-2009.
- Caparrini, F., F. Castelli, and D. Entekhabi (2003), Mapping of land-atmosphere heat fluxes and surface parameters with remote sensing data, *Boundary Layer Meteorol.*, *107*(3), 605–633, doi:10.1023/A:1022821718791.
- Caparrini, F., F. Castelli, and D. Entekhabi (2004a), Estimation of surface turbulent fluxes through assimilation of radiometric surface temperature sequences, *J. Hydrometeorol.*, *5*, 145–159, doi:10.1175/1525-7541(2004)005<0145:EOSTFT>2.0.CO;2.

- Caparrini, F., F. Castelli, and D. Entekhabi (2004b), Variational estimation of soil and vegetation turbulent transfer and heat flux parameters from sequences of multisensor imagery, *Water Resour. Res.*, *40*, W12515, doi:10.1029/2004WR003358.
- Carlson, T. N. (2007), An overview of the “triangle method” for estimating surface evapotranspiration and soil moisture from satellite imagery, *Sensors*, *7*, 1612–1629, doi:10.3390/s7081612.
- Castelli, F., D. Entekhabi, and E. Caporali (1999), Estimation of surface heat flux and an index of soil moisture using adjoint-state surface energy balance, *Water Resour. Res.*, *35*(19), 3115–3125, doi:10.1029/1999WR900140.
- Chehbouni, A., et al. (2008), An integrated modelling and remote sensing approach for hydrological study in arid and semi-arid regions: the SUDMED Program, *Int. J. Remote Sens.*, *29*, 5161–5181, doi:10.1080/01431160802036417.
- Crow, W. T., and W. P. Kustas (2005), Utility of assimilating surface radiometric temperature observations for evaporative fraction and heat transfer coefficient retrieval, *Boundary Layer Meteorol.*, *115*(1), 105–130, doi:10.1007/s10546-004-2121-0.
- De Vries, D. A. (1963), Thermal properties of soils, in *Physics of Plant Environment*, edited by W. R. van Wijk, pp. 210–235, North-Holland Publishing, Amsterdam.
- Dickinson, R. E. (1988), The force-restore model for surface temperatures and its generalizations, *J. Clim.*, *1*(11), 1086–1098, doi:10.1175/1520-0442(1988)001<1086:TFMFST>2.0.CO;2.
- Duchemin, B., et al. (2006), Monitoring wheat phenology and irrigation in Central Morocco: On the use of relationships between evapotranspiration, crops coefficients, leaf area index and remotely-sensed vegetation indices, *Agric. Water Manag.*, *79*, 1–27, doi:10.1016/j.agwat.2005.02.013.
- Gao, Z., R. Horton, L. Wang, H. Liu, and J. Wen (2008), An improved force-restore method for soil temperature prediction, *Eur. J. Soil Sci.*, *59*(5), 972–981, doi:10.1111/j.1365-2389.2008.010600.x.
- Gentine, P., D. Entekhabi, A. Chehbouni, G. Boulet, and B. Duchemin (2007), Analysis of evaporative fraction diurnal behaviour, *Agric. For. Meteorol.*, *143*(1–2), 13–29, doi:10.1016/j.agrformet.2006.11.002.
- Gentine, P., D. Entekhabi and J. Polcher (2010), Spectral behavior of a coupled land and boundary-layer system, *Boundary Layer Meteorol.*, *134*(1), 157–180.
- Gentine, P., J. Polcher, and D. Entekhabi (2011), The diurnal behavior of evaporative fraction in the soil-vegetation-atmospheric boundary layer continuum, *J. Hydrometeorol.*, *12*, 1530–1546, doi:10.1175/2011JHM1261.1.
- Gillies, R. R., T. N. Carlson, J. Cui, W. P. Kustas, and K. S. Humes (1997), A verification of the ‘triangle’ method for obtaining surface soil water content and energy fluxes from remote measurements of the Normalized Difference Vegetation Index (NDVI) and surface radiant temperature, *Int. J. Remote Sens.*, *18*(15), 3145–3166, doi:10.1080/014311697217026.
- Hillel, D. (1998), *Environmental Soil Physics*, Academic Press, London, U. K.
- Hu, Z., and S. Islam (1995), Prediction of ground surface temperature and soil moisture content by the force-restore method, *Water Resour. Res.*, *31*(10), 2531–2539, doi:10.1029/95WR01650.
- Jiang, L. and S. Islam (2001), Estimation of surface evaporation map over Southern Great Plains using remote sensing data, *Water Resour. Res.*, *37*(2), 329–340, doi:10.1029/2000WR900255.
- Kalma, J. D., T. R. McVicar, and M. F. McCabe (2008), Estimating land surface evaporation: A review of methods using remotely sensed surface temperature data, *Surv. Geophys.*, *29*, 421–469, doi:10.1007/s10712-008-9037-z.
- Lhomme, J. P., and E. Elguero (1999), Examination of evaporative fraction diurnal behavior using a soil-vegetation model coupled with a mixed-layer model, *Hydrol. Earth Syst. Sci.*, *3*, 259–270, doi:10.5194/hess-3-259-1999.
- Liu, S., L. Lu, D. Mao, and L. Jia (2007), Evaluating parameterizations of aerodynamic resistance to heat transfer using field measurements, *Hydrol. Earth Syst. Sci.*, *11*, 769–783.
- Mahfouf, J. F., and J. Noilhan (1991), Comparative study of various formulation from bare soil using in situ data, *J. Appl. Meteor.*, *30*(9), 1354–1365, doi:10.1175/1520-0450(1991)030<1354:CSOVFO>2.0.CO;2.
- Mecikalski, J. R., G. R. Diak, M. C. Anderson, and J. M. Norman (1999), Estimating fluxes on continental scales using remotely sensed data in an atmospheric-land exchange model, *J. Appl. Meteor.*, *38*(9), 1352–1369, doi:10.1175/1520-0450(1999)038<1352:EFOSU>2.0.CO;2.
- Monteith, J. L. (1981), Evaporation and surface temperature, *Q. J. R. Meteorol. Soc.*, *107*, 1–27, doi:10.1002/qj.49710745102.
- Moran, M. S., W. P. Kustas, A. Vidal, D. I. Stannard, J. H. Blanford, and W. D. Nichols (1994), Use of ground-based remotely sensed data for surface energy balance evaluation of a semiarid rangeland, *Water Resour. Res.*, *30*, 1339–1349, doi:10.1029/93WR03064.
- Sandholt, I., K. Rasmussen and J. Andersen (2002), A simple interpretation of the surface temperature/vegetation index space for assessment of surface moisture status, *Remote Sens. Environ.*, *79*, 213–224, doi:10.1016/S0034-4257(01)00274-7.
- Santanello, J. A., and M. A. Friedl (2003), Diurnal covariation in soil heat flux and net radiation, *J. Appl. Meteorol.*, *42*, 851–862, doi:10.1175/1520-0450(2003)042<0851:DCISHF>2.0.CO;2.
- Sellers, P. J., F. G. Hall, G. Asrar, D. E. Strebel, and R. E. Murphy (1992), An overview of the First International Satellite Land Surface Climatology Project (ISLSCP) Field Experiment (FIFE), *J. Geophys. Res.*, *97*(D17), 345–371, doi:10.1029/92JD02111.
- Sini, F., G. Boni, F. Caparrini, and D. Entekhabi (2008), Estimation of large-scale evaporation fields based on assimilation of remotely sensed land temperature, *Water Resour. Res.*, *44*, W06410, doi:10.1029/2006WR005574.
- Su, Z. (2002), The Surface Energy Balance System (SEBS) for estimation of turbulent heat fluxes, *Hydrol. Earth Syst. Sci.*, *6*, 85–99, doi:10.5194/hess-6-85-2002.

S. M. Bateni and D. Entekhabi, Ralph M. Parsons Laboratory, Department of Civil and Environmental Engineering, Massachusetts Institute of Technology, 77 Massachusetts Ave., Cambridge, MA 02139, USA. (smbateni@mit.edu; darae@mit.edu)